On the Accurate Evaluation of Intrinsic Electron Mobility on Oxide Semiconductor Transistors

Chen Wang, Longzhong Liao, Kai Jiang, Ziheng Wang, Jinxiu Zhao, *Student Member, IEEE*, Guo Zhou, and Mengwei Si, *Member, IEEE*

***Abstract*— In this work, the evaluation of intrinsic electron mobility (μ) in oxide semiconductor transistors is investigated by different methods. Indium oxide (In_2O_3) transistors with maximum field-effective mobility (μ_{FE_max}) of 97.8 cm ^{2}/Vs were fabricated, where the impact of contact resistance on μ_{FE} was excluded. The μ_{FE}, effective mobility (μ_{eff}) and temperature-dependent Hall mobility (μ_{Hall}) of In_2O_3 transistors are compared. It is found that the deviation of μ_{FE} from μ is caused by the dependence of μ on gate voltages, because of the impact of percolation conduction and surface roughness scattering mechanisms. μ_{eff} and μ_{Hall} align with the global average definition of intrinsic μ, while μ_{FE} characterizes its differential response to gate modulation. Therefore, μ_{eff} and μ_{Hall} are more suitable to represent the intrinsic μ. This work provides a theoretical guideline on the accurate evaluation and further improvement of the mobility of oxide semiconductor transistors.**

***Index Terms*— Oxide semiconductors, mobility, scattering mechanism.**

I. Introduction

OXIDE semiconductor transistors have been widely adopted in display technologies and are considered as the promising candidate for monolithic 3D applications, benefiting from their low leakage current, high mobility, steep subthreshold swing and low thermal budget [1], [2]. Indium-rich oxide semiconductors by atomic layer deposition (ALD), such as indium oxide (In_2O_3) [3], [4], indium tin oxide (ITO). [4], indium tungsten oxide (IWO) [5], indium zinc oxide (IZO) [6], indium gallium zinc oxide (IGZO) [7], [8], etc., have been reported achieving high mobility. However, in literature, field-effect mobility (μ_{FE}) is commonly used to represent the intrinsic mobility (μ), which is often overestimated. In many cases, this overestimation is a result of artifacts arising from non-ideal contacts, as reported in [9] and [10].

Received 1 August 2025; revised 22 August 2025; accepted 27 August 2025. Date of publication 2 September 2025; date of current version 24 October 2025. This work was supported in part by STI 2030-Major Projects under Grant 2022ZD0210600, in part by the National Natural Science Foundation of China under Grant 62274107 and Grant 92264204, and in part by Shanghai Pilot Program for Basic Research-Shanghai Jiao Tong University under Grant 21TQ1400212. The review of this letter was arranged by Editor S. Zhang. *(Corresponding author: Mengwei Si.)*

Chen Wang, Kai Jiang, Ziheng Wang, Jinxiu Zhao, and Mengwei Si are with the State Key Laboratory of Micro-Nano Engineering Science and the School of Information Science and Electronic Engineering, Shanghai Jiao Tong University, Shanghai 200240, China (e-mail: mengwei.si@sjtu.edu.cn).

Longzhong Liao and Guo Zhou are with the 13th Research Institute, CETC, Shijiazhuang 050051, China.

Digital Object Identifier 10.1109/LED.2025.3604471

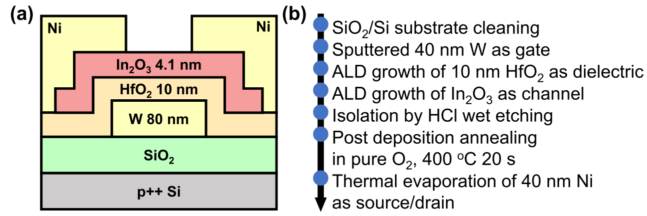

Fig. 1. (a) Schematic diagram of an In_2O_3 transistor with 10 nm HfO_2 as insulator and T_{ch} of 4.1 nm. (b) Fabrication process flow of the bottom-gate In_2O_3 transistor.

For the high mobility oxide semiconductor transistors with good ohmic contact, the μ_{FE} may still be overestimated. The μ_{FE} is typically extracted from the transconductance (g_m) of transfer curves, where μ_{FE} first increases to its maximum value (μ_{FE_max}) and then rapidly decreases with gate-to-source voltage (V_{GS}), which is far less than the effective mobility (μ_{eff}). Therefore, the usage of μ_{FE} to evaluate the μ of oxide semiconductor transistors may not be reliable. However, the physical origin of the deviation has been ignored and has not been understood.

In this work, In_2O_3 transistors with high μ_{FE} are fabricated. Ohmic contacts are formed at source/drain (S/D) with post-deposition annealing process, so that the influence of S/D contacts on mobility evaluation can be excluded. μ_{FE}, μ_{eff} and Hall mobility (μ_{Hall}) measurements are performed. It is found μ_{FE} in oxide semiconductor transistors deviates from μ because of the V_{GS}-dependence of μ, leading to the overestimation at low V_{GS} and underestimation at high V_{GS}. Therefore, μ_{eff} and μ_{Hall} are more suitable to evaluate the intrinsic μ. Moreover, the dependence of μ on V_{GS} is found to likely originates from the percolation conduction and surface roughness scattering mechanisms.

II. Experiments

Fig. 1(a) shows the schematic diagram of a back-gate In_2O_3 transistor in this work. The device fabrication process is summarized in Fig. 1(b). 80 nm W gate was deposited by magnetron sputtering. 10 nm HfO_2 insulator was grown by ALD at 200 °C. In_2O_3 channel was grown by ALD at 225 °C. Post-deposition annealing was carried out in O_2 at 400 °C for 20 s. 40 nm Ni S/D electrodes were deposited by thermal evaporation. The thickness of In_2O_3 (T_{ch}) was determined by atomic force microscopy (AFM). Electrical characterization was done at room temperature in vacuum under ~5 Pa. I-V and C-V were completed by Keysight B1500 and E4980, respectively. Hall bar devices were fabricated together with

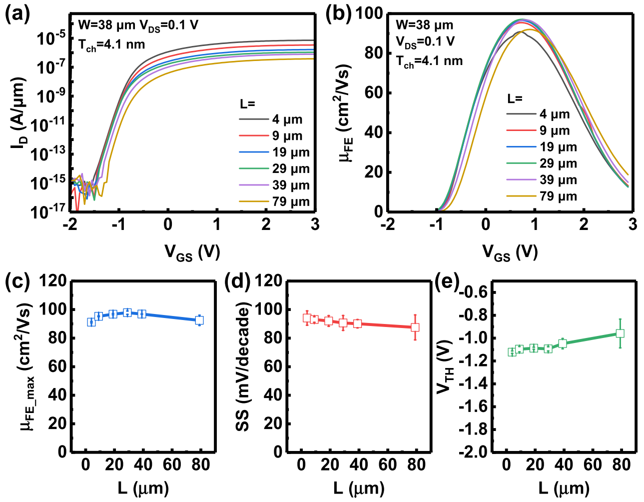

Fig. 2. (a) Transfer curves and (b) extracted μ_{FE} at V_{DS} of 0.1 V of In_2O_3 transistors with T_{ch} of 4.1 nm and different L. (c)-(e) L-dependent μ_{FE_max}, SS and V_{TH} of In_2O_3 transistors. Each data point represents the average of 3 different devices.

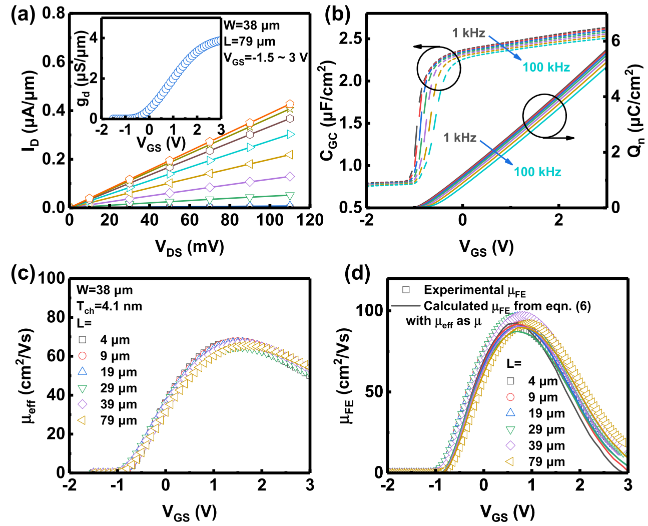

Fig. 3. (a) Output curves of an In_2O_3 transistor with T_{ch} of 4.1 nm. The inset is the g_d versus V_{GS} characteristics. (b) C_{GC} and the corresponding Q_n versus V_{GS} characteristics. The frequency varies from 1 kHz to 100 kHz. (c) μ_{eff} of In_2O_3 transistors with different L. The C_{GC} is acquired at 1 kHz. (d) Comparison between experimental μ_{FE} and that calculated from μ_{eff}.

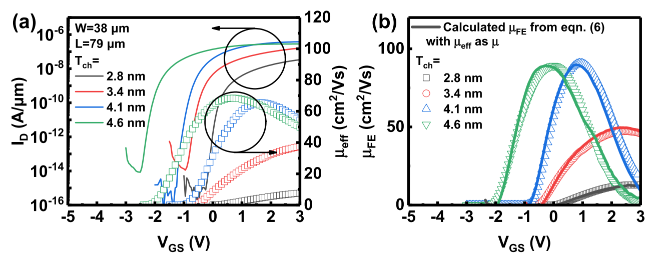

Fig. 4. (a) Transfer curves, μ_{eff} and (c) experimental μ_{FE} and that calculated from μ_{eff} of In_2O_3 transistors with different T_{ch}.

transistors to evaluate μ_{Hall} and sheet carrier density (n_{sheet}) with channel length (L) of 200 μm and channel width (W) of 60 μm. The Hall measurement was carried out in a physical property measurement system (PPMS) (DynaCool-14T).

III. Results and Discussion

Fig. 2(a) presents the transfer curves of In_2O_3 transistors with different L. The drain current (I_D) in linear region ($V_{DS} \ll V_{GS}$-V_{TH}) can be written as [11]

$$I_D = \frac{W}{L}\mu Q_n V_{DS} = \frac{W}{L}\mu C_{ox}\left(V_{GS} - V_{TH} - \frac{V_{DS}}{2}\right)V_{DS} \tag{1}$$

where Q_n is the mobile carrier density, C_{ox} is the gate capacitance, V_{TH} is the threshold voltage, and V_{DS} is the drain-to-source voltage. The μ_{FE} is defined using g_m [11]

$$\mu_{FE} = \frac{L}{WC_{ox}V_{DS}}\left(\frac{\partial I_D}{\partial V_{GS}}\right) = \frac{g_m L}{WC_{ox}V_{DS}} \tag{2}$$

However, the definition of μ_{FE} deviates from the physical definition of μ, which is $\mu = \sigma/qn_e$, where σ is the conductivity, q is the electron charge and n_e is the carrier density. The μ calculated from $\mu = \sigma/qn_e$ is consistent with the basic definition of intrinsic μ, which describes the "average mobility" of carriers at conduction band. Eqn. (2) is only achieved by assuming μ is constant, that is, $\mu = \mu_{FE} = \partial\sigma/q\partial n_e$. μ_{FE} of devices in Fig. 2(a) is extracted as shown in Fig. 2(b). μ_{FE} increases to μ_{FE_max} and then rapidly drops. Transistors with different L have similar μ_{FE}, suggesting that good ohmic contacts are formed at S/D. Therefore, the peak in μ_{FE}-V_{GS} characteristics is unrelated with contact resistance. The extracted μ_{FE_max}, SS and V_{TH} scaling metrics are plotted in Fig. 2(c)-2(e). The devices exhibit a high on/off ratio > 10^{10}, a high μ_{FE_max} of 97.8 cm^2/Vs, a SS of ~90 mV/decade, and a V_{TH} of ~-1 V. The contact resistance (R_C) is extracted by the transfer length method (TLM), which is much lower than total resistance (R_{tot}) at V_{GS} from −2 V to 3 V. It suggests that an excellent ohmic contact is formed and the R_C will not have an obviously impact on the transfer characteristics. It is also confirmed that μ_{FE} extracted in linear region does not change with V_{DS}, so the laterally field will not affect μ_{FE} for In_2O_3 transistors with L > 1 μm.

μ_{eff} is typically defined by [11]

$$\mu_{eff} = \frac{L}{WQ_n}\frac{\partial I_D}{\partial V_{DS}} = \frac{Lg_d}{WQ_n} \tag{3}$$

where g_d is the drain conductance. The definition of μ_{eff} conforms to the physical definition of intrinsic μ. The Q_n is typically acquired from the integral of gate-to-channel capacitance (C_{GC}) by C-V measurements, where Q_n can be written as [11]

$$Q_n = \int_{-\infty}^{V_{GS}} C_{GC}\,dV_{GS} \tag{4}$$

It is more reliable than to calculate Q_n using $C_{ox}(V_{GS}$-$V_{TH})$, because it avoids the uncertainty around V_{TH}. Fig. 3(a) shows the output curves of In_2O_3 transistors with V_{GS} from −1.5 V to 3 V and V_{DS} from 0 mV to 110 mV. The devices are in linear region due to the relatively small V_{DS}. The g_d extracted from output curves is plotted in the inset of Fig. 3(a). Fig. 3(b) shows the C_{GC} and the corresponding Q_n of In_2O_3 transistors with S/D electrodes grounded. The frequency dispersion of C_{GC} is likely due to electron generation and recombination from the subgap defect states [12]. C_{GC} measured at low frequency is adopted to extract the μ_{eff}. Fig. 3(c) shows the

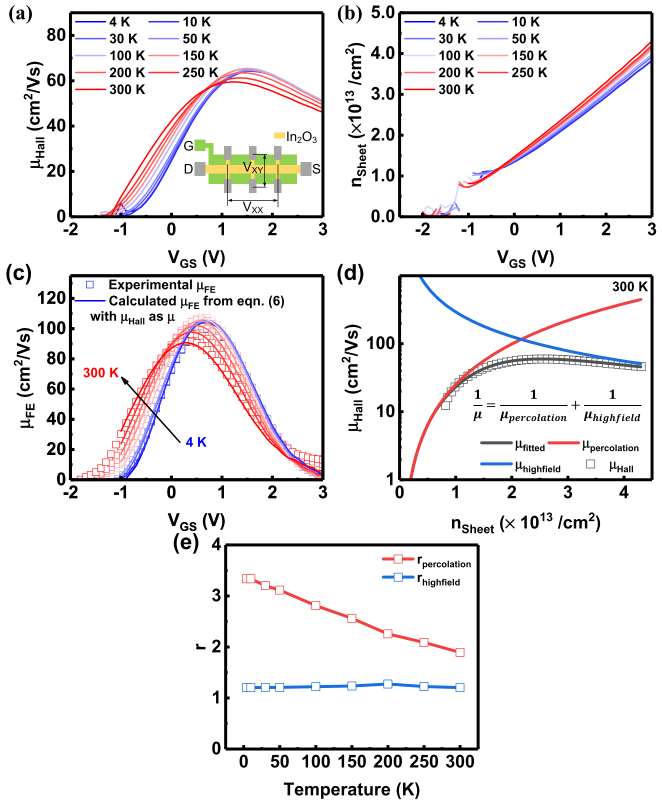

Fig. 5. (a) μ_{Hall} and (b) n_{sheet} versus V_{GS} characteristics from 4 K to 300 K of an In_2O_3 device with T_{ch} of 4.1 nm. (c) Comparison between the experimental μ_{FE} in Hall bar and that calculated from μ_{Hall} using eqn. (6) at 4 K ~ 300 K. (d) Numerical fitting of μ_{Hall} verus n_{sheet} characteristics at 300 K by percolation and high field scattering mechanisms. (e) Temperature-dependent $r_{percolation}$ and $r_{highfield}$ from 4 K to 300 K.

μ_{eff} of In_2O_3 transistors with different L. The maximum μ_{eff} is ~65 cm^2/Vs, which is smaller than μ_{FE_max}. The decrease of μ_{eff} under high V_{GS} is also smaller than that of μ_{FE}. The reason for the difference between μ_{FE} and μ_{eff} is because the dependence of μ on V_{GS} is ignored when calculating μ_{FE} in eqn. (2), where

$$\frac{\partial I_D}{\partial V_{GS}} = \frac{W C_{ox} V_{DS}}{L} \frac{\partial}{\partial V_{GS}} \left(\mu \left(V_{GS} - V_{TH} - \frac{V_{DS}}{2} \right) \right) \quad (5)$$

By combining eqn. (2) and (5), the μ_{FE} can be written as

$$\mu_{FE} = \frac{\partial \mu}{\partial V_{GS}} \left(V_{GS} - V_{TH} - \frac{V_{DS}}{2} \right) + \mu \quad (6)$$

In general, μ_{FE} is close to μ because $\partial\mu/\partial V_{GS}$ can be ignored, such as in the case of silicon. However, in oxide semiconductor transistors, the existence of $\partial\mu/\partial V_{GS}$ will cause a large error when evaluating μ by μ_{FE}, which might be caused by percolation or other scattering mechanism.

According to the definition of μ_{eff} in eqn. (3), there is no derivative to V_{GS}, so it is closer to μ. If μ_{eff} is used as μ in eqn. (6), the corresponding μ_{FE} can be calculated. Fig. 3(d) compares the experimental μ_{FE} and that calculated from eqn. (6) with μ_{eff} as μ in transistors with different L. The experimental μ_{FE} and that calculated with μ_{eff} as μ match well for all devices, which further confirms that the overestimation of μ_{FE_max} is caused by the dependence of μ on V_{GS}. The transfer curves, μ_{eff}, experimental μ_{FE} and that calculated from μ_{eff} of In_2O_3 transistor with different T_{ch} are plotted in Figs. 4(a) and (b), respectively. For In_2O_3 transistors with different T_{ch}, the experimental μ_{FE} and that calculated from μ_{eff} match well, which further confirms that μ_{eff} represents the intrinsic μ more accurately.

Hall effect measurement is a widely adopted approach to measure the μ_{Hall} and n_{sheet}. Figs. 5(a) and (b) present the μ_{Hall} and n_{sheet} at temperatures from 4 K to 300 K. μ_{Hall} exhibits the similar relation with V_{GS} as μ_{eff}. μ_{FE} is also extracted from the Hall bar, where the impact of R_C can be avoided using a 4-point approach, so that it is more accurate than that in a transistor. Fig. 5(c) gives the experimental μ_{FE} and that calculated according to eqn. (6) with μ_{Hall} as μ at 4 K ~ 300 K, which match better than that calculated with μ_{eff} as μ. The μ_{FE_max} corresponds to peak $d\sigma/dn$ values during new conductive channel formation, confirming its origin as a fundamental physical feature of carrier transport in oxide semiconductor. It also confirms that μ_{Hall} can better represents the μ of In_2O_3 transistors than μ_{eff}, because Hall measurements directly measure the n_{sheet} so that it can avoid the error caused by frequency dispersion in C-V.

To furtherly investigate the dependence of μ on V_{GS}, Fig. 5(d) depicts μ_{Hall} verus n_{sheet} characteristics of In_2O_3 transistors at 300 K. Note that n_{sheet} increases linearly with V_{GS}, suggesting the fast decrease of μ_{FE} at high V_{GS} is not because of the overestimation of free carrier density by C_{OX}, also indicating a low trap density at high V_{GS}. At low carrier density ($n_{sheet} < 2 \times 10^{13}$ /cm^2), μ_{Hall} increases with n_{sheet}, which is likely caused by percolation mechanism [13] and trap-limited conduction [14]. At high carrier density $n_{sheet} > 2 \times 10^{13}$ /cm^2, μ_{Hall} decreases with n_{sheet} because of the high field scattering due to surface roughness or phonon, as described by $\mu_{highfield} = \mu_{h0} (n_{sheet}/n_{h0})^{-r_{highfield}}$, where μ_{h0}, n_{h0} and $r_{highfield}$ are fitting parameters. In Fig. 5(d), μ_{Hall} verus n_{sheet} characteristics at 300 K is fitted by percolation conduction and high field scattering according to Matthiessen's rule, i.e., $\mu_{Hall}^{-1} = \mu_{percolation}^{-1} + \mu_{highfield}^{-1}$. The mobility limited by percolation is $\mu_{percolation} = \mu_{p0} \left(n_{sheet}/n_{p0}\right)^{-r_{percolation}}$, where μ_{p0}, n_{p0}, and $r_{percolation}$ are fitting parameters [13]. It is found that the percolation conduction and high field scattering can match well with the experimental results. The μ_{Hall} verus n_{sheet} characteristics from 4 K to 300 K are also fitted (data not shown), and the corresponding $r_{percolation}$ and $r_{highfield}$ are plotted in Fig. 5(e). $r_{percolation}$ decreases at high temperature, consistent with the thermal activation characteristics of the percolation conduction [13], [15]. For high field scattering, when $r_{highfield}$ is equal to 0.3, it corresponds to phonon scattering, while when r is 2, it corresponds to surface roughness scattering [16]. The fitted $r_{highfield}$ of ~1.2 hardly changes with temperature. Therefore, surface roughness scattering is likely to be the dominant high field scattering mechanism.

IV. Conclusion

In conclusion, the overestimation of μ by μ_{FE_max} in oxide semiconductor is well explained by the dependence of μ on V_{GS}, due to the percolation conduction and surface roughness scattering related mechanisms. It is proposed that μ_{eff} and μ_{Hall} can better represent μ compared with μ_{FE}. The reported μ_{FE} and its engineering methods in literature may need to be revisited.

References

[1] K. Nomura, H. Ohta, A. Takagi, T. Kamiya, M. Hirano, and H. Hosono, "Room-temperature fabrication of transparent flexible thin-film transistors using amorphous oxide semiconductors," *Nature*, vol. 432, no. 7016, pp. 488–492, Nov. 2004, doi: 10.1038/nature03090.

[2] X. Duan, K. Huang, J. Feng, J. Niu, H. Qin, S. Yin, G. Jiao, D. Leonelli, X. Zhao, Z. Wang, W. Jing, Z. Wang, Y. Wu, J. Xu, Q. Chen, X. Chuai, C. Lu, W. Wang, G. Yang, D. Geng, L. Li, and M. Liu, "Novel vertical channel-all-around (CAA) In-Ga-Zn-O FET for 2T0C-DRAM with high density beyond $4F^2$ by monolithic stacking," *IEEE Trans. Electron Devices*, vol. 69, no. 4, pp. 2196–2202, Apr. 2022, doi: 10.1109/TED.2022.3154693.

[3] M. Si, Z. Lin, Z. Chen, X. Sun, H. Wang, and P. D. Ye, "Scaled indium oxide transistors fabricated using atomic layer deposition," *Nature Electron.*, vol. 5, no. 3, pp. 164–170, Feb. 2022, doi: 10.1038/s41928-022-00718-w.

[4] K. Han, Y. Kang, X. Chen, Y. Chen, and X. Gong, "Indium-tin-oxide thin-film transistors with high field-effect mobility (129.5 cm^2/Vs) and low thermal budget (150 °C)," *IEEE Electron Device Lett.*, vol. 44, no. 12, pp. 1999–2002, Dec. 2023, doi: 10.1109/LED.2023.3329481.

[5] W. Chakraborty, B. Grisafe, H. Ye, I. Lightcap, K. Ni, and S. Datta, "BEOL compatible dual-gate ultra thin-body W-doped indium-oxide transistor with Ion = 370 μA/μm, SS = 73 mV/dec and I_{on}/I_{off} ratio > 4×10^9," in *Proc. IEEE Symp. VLSI Technol.*, Jun. 2020, Paper TH2.1, doi: 10.1109/VLSITECHNOLOGY18217.2020.9265064.

[6] H.-M. Kim, S.-H. Ryu, S. Kim, K.-H. Lee, and J.-S. Park, "C-axis aligned composite InZnO via thermal atomic layer deposition for 3D nanostructured semiconductor," *ACS Appl. Mater. Interfaces*, vol. 16, no. 12, pp. 14995–15003, Mar. 2024, doi: 10.1021/acsami.3c16879.

[7] J. Sheng, T. Hong, H.-M. Lee, K. Kim, M. Sasase, J. Kim, H. Hosono, and J.-S. Park, "Amorphous IGZO TFT with high mobility of 70 cm^2/(Vs) via vertical dimension control using PEALD," *ACS Appl. Mater. Interfaces*, vol. 11, no. 43, pp. 40300–40309, Oct. 2019, doi: 10.1021/acsami.9b14310.

[8] S. Samanta, U. Chand, S. Xu, K. Han, Y. Wu, C. Wang, A. Kumar, H. Velluri, Y. Li, X. Fong, A. V.-Y. Thean, and X. Gong, "Low subthreshold swing and high mobility amorphous indium-gallium-zinc-oxide thin-film transistor with thin HfO_2 gate dielectric and excellent uniformity," *IEEE Electron Device Lett.*, vol. 41, no. 6, pp. 856–859, Jun. 2020, doi: 10.1109/LED.2020.2985787.

[9] D. J. Gundlach, L. Zhou, J. A. Nichols, T. N. Jackson, P. V. Necliudov, and M. S. Shur, "An experimental study of contact effects in organic thin film transistors," *J. Appl. Phys.*, vol. 100, no. 2, Jul. 2006, Art. no. 024509, doi: 10.1063/1.2215132.

[10] C. Wang, C. Zeng, W. Lu, H. Ning, F. Li, and F. Ma, "High performance Schottky barrier TFTs with indium-gallium-zinc-oxide/Mo Schottky junction," *IEEE Electron Device Lett.*, vol. 44, no. 4, pp. 646–649, Apr. 2023, doi: 10.1109/LED.2023.3244583.

[11] D. K. Schroder, *Semiconductor Material and Device Characterization*. Hoboken, NJ, USA: Wiley, 2006, doi: 10.1002/0471749095.

[12] Z. Wang, Z. Lin, M. Si, and P. D. Ye, "Characterization of interface and bulk traps in ultrathin atomic layer-deposited oxide semiconductor MOS capacitors with HfO_2/In_2O_3 gate stack by C-V and conductance method," *Frontiers Mater.*, vol. 9, May 2022, Art. no. 850451, doi: 10.3389/fmats.2022.850451.

[13] K. Abe, A. Sato, K. Takahashi, H. Kumomi, T. Kamiya, and H. Hosono, "Mobility- and temperature-dependent device model for amorphous In-Ga-Zn-O thin-film transistors," *Thin Solid Films*, vol. 559, pp. 40–43, May 2014, doi: 10.1016/j.tsf.2013.11.066.

[14] M. J. Kim, H. J. Park, S. Yoo, M. H. Cho, and J. K. Jeong, "Effect of channel thickness on performance of ultra-thin body IGZO field-effect transistors," *IEEE Trans. Electron Devices*, vol. 69, no. 5, pp. 2409–2416, May 2022, doi: 10.1109/TED.2022.3156961.

[15] K. Abe, K. Takahashi, A. Sato, H. Kumomi, K. Nomura, T. Kamiya, and H. Hosono, "Operation model with carrier-density dependent mobility for amorphous In-Ga-Zn-O thin-film transistors," *Thin Solid Films*, vol. 520, no. 10, pp. 3791–3795, Mar. 2012, doi: 10.1016/j.tsf.2011.10.060.

[16] S. Takagi, A. Toriumi, M. Iwase, and H. Tango, "On the universality of inversion layer mobility in Si MOSFET's: Part I-effects of substrate impurity concentration," *IEEE Trans. Electron Devices*, vol. 41, no. 12, pp. 2357–2362, Dec. 1994, doi: 10.1109/16.337449.